Volume 21 | Issue 1 Article 4

2022

Use of InSAR in Linear Discontinuous Ground Deformation Generation Analysis: Case Study of a Mine in Poland

Author(s) ORCID Identifier:
Bartosz Apanowicz 0000-0002-7268-8786

Use of InSAR in Linear Discontinuous Ground Deformation Generation Analysis: Case Study of a Mine in Poland

Abstract

Linear Discontinuous Ground Deformations are defined as fissures and steps, as well as structural forms composed of them. They occur on the surface as a result of underground mining. Knowledge of LDGDs has been acquired through field observations which are subsequently described in the scientific publication. Records of LDGDs are made by using the classic surveying method. The paper reviews the created LDGDs in the years 2015–2019 in one of the mines of the USCB. The analysis covers the velocity of subsidence as a result of underground mining and the values of horizontal strains determined according to the Knothe-Budryk theory. The InSAR satellite technique was used to measure the subsidence. The subsidence was determined using the small baseline method – SBAS. The combination of the theoretical Knothe-Budryk model with the large-scale capabilities of InSAR may provide valuable material for a better understanding of the genesis of LDGD creation and their prediction.

Keywords

underground mining, subsidence, horizontal strains, Knothe-Budryk theory, satellite interferometry, SBAS method

Use of InSAR in linear discontinuous ground deformation generation analysis: Case study of a mine in Poland

Bartosz Apanowicz

Central Mining Institute, Department of Geology, Geophysics and Surface Protection, Katowice, Poland

Abstract

Linear Discontinuous Ground Deformations are defined as fissures and steps, as well as structural forms composed of them. They occur on the surface as a result of underground mining. Knowledge of LDGDs has been acquired through field observations which are subsequently described in the scientific publication. Records of LDGDs are made by using the classic surveying method. The paper reviews the created LDGDs in the years 2015−2019 in one of the mines of the USCB. The analysis covers the velocity of subsidence as a result of underground mining and the values of horizontal strains determined according to the Knothe-Budryk theory. The InSAR satellite technique was used to measure the subsidence. The subsidence was determined using the small baseline method − SBAS. The combination of the theoretical Knothe-Budryk model with the large-scale capabilities of InSAR may provide valuable material for a better understanding of the genesis of LDGD creation and their prediction.

Keywords: underground mining, subsidence, horizontal strains, Knothe-Budryk theory, satellite interferometry, SBAS method

1. Introduction

All underground mining exploitation results in natural environment degradation on the surface. Its consequences include mining-induced deformations that may manifest themselves in continuous or discontinuous forms. Discontinuous deformations are known as linear discontinuous ground deformations (LDGDs), and they typically manifest themselves as steps and fissures, as well as structural forms composed of them, including stairs, horsts and ditches [1]. Their occurrence in urban areas is particularly hazardous, as it may lead to structure and traffic infrastructure damage. Examples of LDGDs are presented in Fig. 1.

Knowledge of LDGDs is acquired through field observations of occurring cases, which are subsequently described in scientific publications. Examples include mine monographs [2,3]. The first descriptions of discontinuous deformation generation as a result of hard coal mining, at a depth of 300 m, were provided in 1939 by Klenczar [4]. Today, the issue is investigated by scientists of the Silesian University of Technology (Gliwice, Poland) [5]. The latest research proves that discontinuities may occur as a result of deep mining, and that LDGD generation is influenced by the time between individual mining activities, as well as by the face advance rate [6]. Grün has made a significant contribution to the understanding of the mechanisms that accompany LDGD generation [7]. Based on an analysis of nearly 1200 cases, he presented the first method for discontinuous deformation forecasting. Grün's research was an inspiration to the scientists of the Central Mining Institute (Katowice, Poland), where two methods for determining the likelihood of LDGD generation were developed in the years 2006−2009 [1,8]. Nevertheless, LDGD forecasting is yet to be described using a reliable theory. In recent years, cases of LDGDs have also been observed in Chinese hard coal mining [9]. It was also demonstrated that the width of the generated fissures is directly proportional to the value of horizontal strain [10]. Records of LDGDs are kept by the measuring and geological departments of mining

Received 18 January 2022; revised 23 March 2022; accepted 24 March 2022.
Available online 30 April 2022
E-mail address: bapanowicz@gig.eu.

https://doi.org/10.46873/2300-3960.1346

Fig. 1. Examples of linear discontinuous ground deformations (LDGDs).

plants. The measurements are conducted using classic surveying methods.

With the development that satellite measurement methods have witnessed over the years, they have become a good complement to the classic geodesic methods. These include such solutions as InSAR satellite interferometry. It is a remote sensing technique utilising satellites equipped with radars with synthetic apparatus [11]. It finds broad application in measuring the natural movements of the surface of the Earth [12–15], flooding effects [16] and earthquakes [17,18]. It is also successfully used for determining subsidence troughs generated as a result of mining activity. It is applied in both international [19,20] and Polish mining [21–23]. In the context of discontinuous deformations, the latest research presents attempts at detecting LDGDs using the coherence of two pairs of satellite images [24].

The purpose of this article is to present LDGDs generated over the years 2015–2019 in the light of measurements conducted with InSAR satellite interferometry. The article includes an analysis of surface subsidence velocities determined using the InSAR method in the context of LDGD generation. The satellite measurements were complemented with an analysis of horizontal strains determined according to the Knothe-Budryk theory [25,26]. The large quantity of data provided by the InSAR technology compared with classic geodesic measurements, complemented with theoretical assumptions, may constitute valuable material for analysing the generation of discontinuous deformations and also contribute to the better forecasting of their occurrence. Case study: one of the mines in the Upper Silesian Coal Basin in Poland.

2. Materials and methods

2.1. Description of linear discontinuous ground deformations (LDGDs)

The analysis was conducted based on the experience of a mining plant in the Upper Silesian Coal Basin in Poland. In the years 2015–2019, 78 documented cases of discontinuous deformations

Table 1. Descriptions of LDGDs divided into groups.

Group	Date of measurement	Type of LDGD	Description
1	08.2015	3 × step	h = 0.3–0.5 m
	03.2019	1 × step	h = 0.1 m
2	10.2015	3 × fissure	–
		2 × step	h = 0.4–0.5 m
3	04.2016	9 × fissure	–
		3 × step	h = 0.05–0.4 m
4	08.2016	7 × fissure	–
5	09.2016	12 × fissure	–
		2 × graben	–
		1 × sinkhole	–
6	03.2017	4 × fissure	–
		3 × step	h = 0.2–0.25 m
	02.2019	2 × step	h = 0.1–0.2 m
7	03.2017	8 × step	h = 0.1 m
8	07.2017	2 × step	h = 0.1–0.4 m
	12.2018	1 × step	h = 0.1 m
9	07.2017	2 × step	h = 0.1–0.2 m
	08.2017	1 × step	h = 0.2 m
10	12.2018	2 × step	h = 0.1–0.15 m
11	03.2019	2 × step	h = 0.1 m
12	08.2019	8 × step	h = 0.1–0.4

appeared as a result of mining activity. The deformations had the form of terraces with a fault throw h = 0.05–0.5 m, of fissures, steps and grabens. They can be divided into 12 groups based on the measurement date and the location of occurrence, and their descriptions are presented in Table 1. The locations of individual deformation groups are presented in Fig. 2.

2.2. Geological and mining conditions

Mining in the area of the generated LDGDs was conducted in five coal seams in 15 longwalls. Caving was used as the roof control system. The mining depth was 350–760 m, whereas the height of the individual longwalls was 1.6–4.0 m. Detailed information regarding the geological and mining conditions is presented in Table 2.

Table 2 demonstrates that mining began in May 2014, in longwall C-3 in coal seam 503-4, and ended in June 2020, in longwall C-1 in the bottom stratum of coal seam 505. All the LDGDs occurred in the area of the boundaries of individual longwalls, as presented in Fig. 3.

2.3. InSAR data

Surface subsidence was determined using the SBAS (Small Baseline Subset) time-series method [27]. The method involves interferograms generated

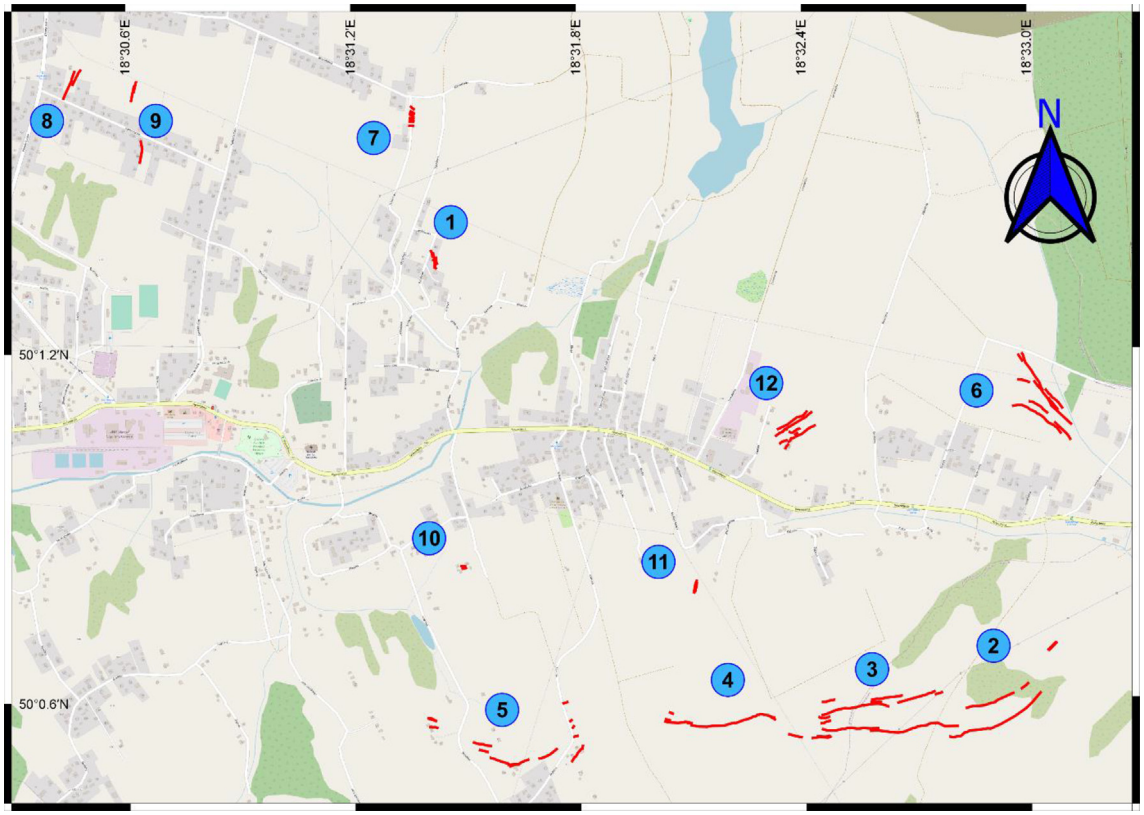

Fig. 2. Locations of LDGDs (red lines) divided into groups (blue circles).

Table 2. Detailed information about underground coal mining.

Seam	Longwall	Mean height [m]	Mean depth [m]	Inclination [°]	Start date	End date	Roof development
503–4	C-3	3.6	621	9	05.2014	12.2015	Cave-in
	C-4	3.6	648	8	02.2019	10.2020	Cave-in
505 top layer	C-2	2.5	470	14	06.2015	10.2015	Cave-in
	W-5	3.0 °	364	14	11.2014	07.2016	Cave-in
	C-7	3.0	459	14	12.2015	03.2016	Cave-in
	C-3	3.0	622	17	04.2016	03.2017	Cave-in
	C-5a	3.0	348	9	07.2016	12.2016	Cave-in
	W-6	3.0	410	13	11.2016	01.2018	Cave-in
	C-4	3.0	684	19	11.2017	04.2019	Cave-in
	W-7	3.0	460	15	10.2018	01.2020	Cave-in
507	W-3	4.0	365	9	07.2017	11.2017	Cave-in
	C-2	3.8	353	10	04.2018	11.2018	Cave-in
502/2	C-4	1.7	726	16	01.2017	08.2017	Cave-in
	C-6	1.6	757	7	02.2018	08.2018	Cave-in
505 bottom layer	C-1	3.0	513	15	08.2019	06.2020	Cave-in

from sets of images selected based on an adopted baseline and timeline. Afterwards, deformations in the direction of the LOS (line of sight) are calculated from the set of interferograms. The baseline is the perpendicular distance between two passes of the satellite. The timeline is the temporal distance between subsequent passes of the satellite.

The deformations were determined using 229 images taken by the Sentinel-1 satellite of the European Space Agency (ESA). The satellite moved along the descending orbit no. 51. The images were taken over the period of January 2015 to December 2019. Initially, until September 2016, the revisit time was 12 days (Sentinel-1A satellite), and in the later period it was six days (Sentinel-1A/1B). A distance of 100 m was adopted as the baseline limit, and 50 days as the timeline limit. A 100 m wave filter length was used during the interferogram filtering,

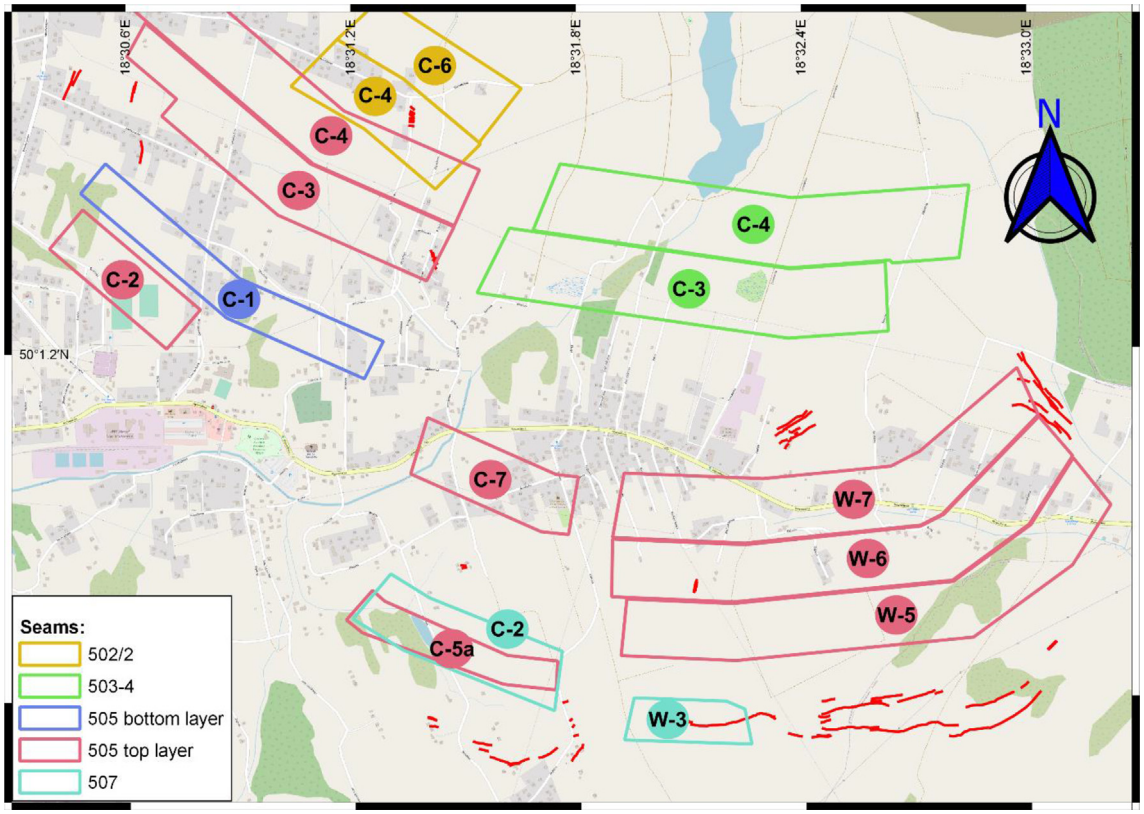

Fig. 3. Longwall locations in relation to LDGDs.

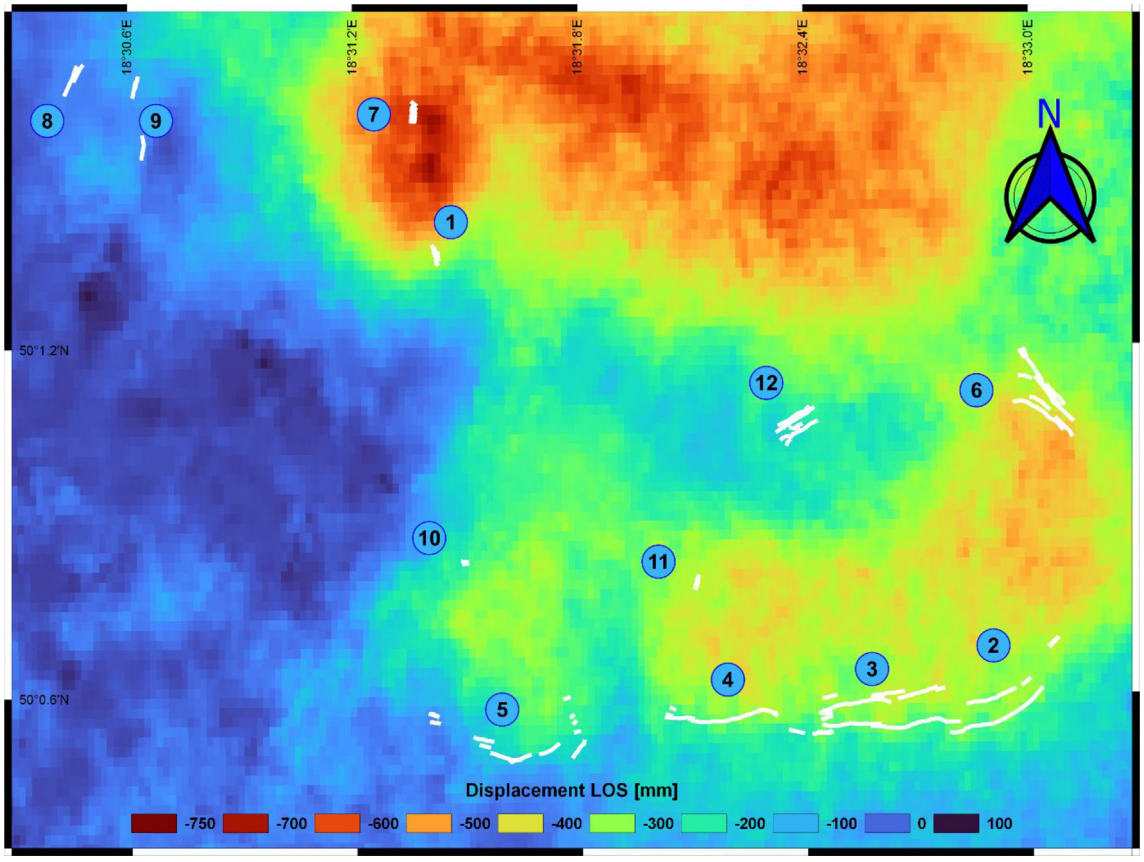

Fig. 4. Subsidence caused by the analysed underground mining over the period of 01.2015–08.2019, determined per the InSAR method, with LDGD locations (white colour).

as well as a decimation factor of 8 for range and 2 for azimuth. The process utilised two-dimensional phase unwrapping [28]. The GMTSAR software was used for the calculations [29]. The results yielded the surface subsidence process for the period of 2015–2019.

3. Results and discussion

3.1. LDGD location analysis

Figure 4 presents the surface subsidence in the direction of the LOS obtained from the InSAR analysis, together with the locations of the generated discontinuous deformations. The depicted subsidence is the result of the analysed underground mining activity (Fig. 3) over the period of January 2015 to August 2019 – the date of the occurrence of the final discontinuous deformation.

The greatest LOS subsidence did not exceed 750 mm. Fig. 3 presented in Section 2 demonstrates that all the LDGDs appeared on the boundaries of extraction. This is also confirmed by Fig. 4, where it can be observed that most of the LDGDs occurred on the borders of subsidence troughs, i.e. in the areas of the greatest horizontal tensile strains. To confirm this, horizontal tensile strains were determined according to the Knothe-Budryk theory [25,26] for the period from the date the analysed mining activity began – May 2014 – to the appearance of the final discontinuous deformation – August 2019. The SZKODY 5.0 software developed at the Central Mining Institute was used for the calculations [30]. The following theoretical parameters were adopted based on the experience of the mining plant conducting the extraction:

- extraction coefficient $a = 0.85$,
- rock mass parameter tg $\beta = 2.0$,
- coefficient of influence deviation $k = 0.7$.

The calculation results are presented in Fig. 5.

The greatest horizontal strains were located in the area of group 5, with LDGDs of up to 10 mm/m, and in the area of group 12, with LDGDs of about 6 mm/m. The lowest horizontal strains were located in the area of groups 2 and 3 and ranged from 0 to 4 mm/m. The actual strain range may have been greater, which is confirmed by the range of the subsidence trough (in the areas of LDGD

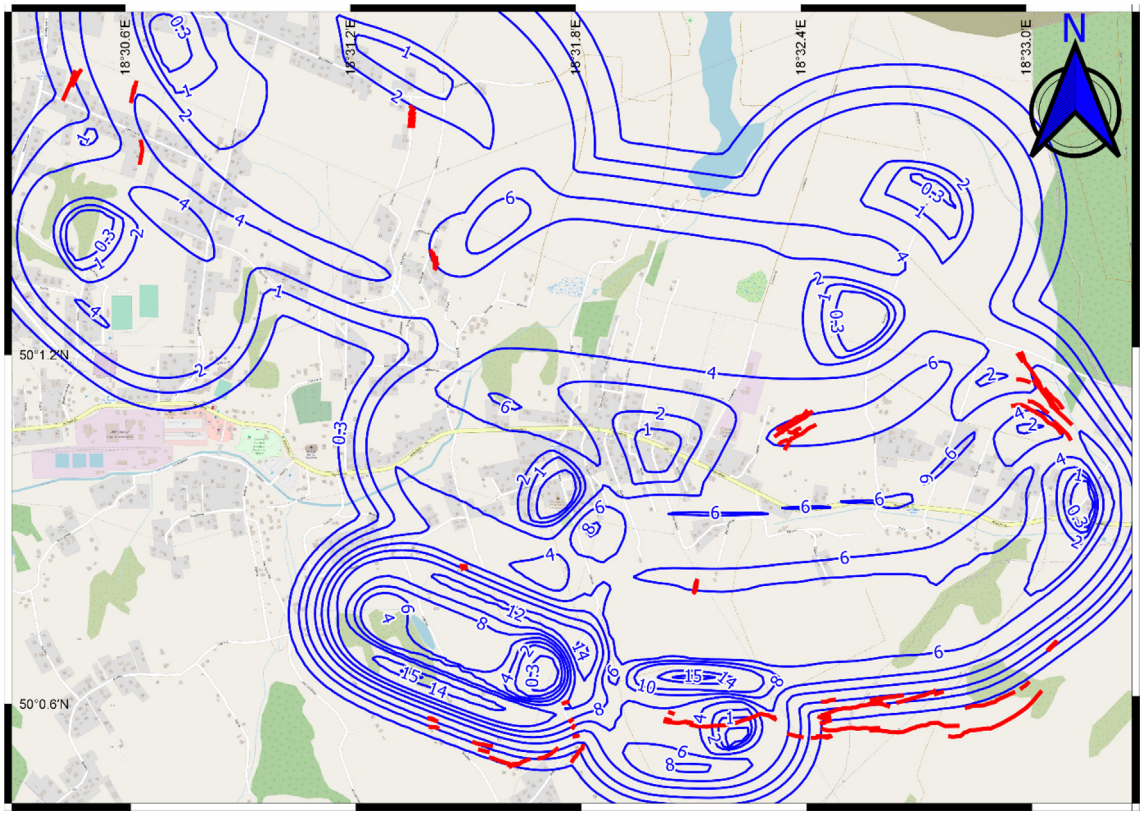

Fig. 5. Horizontal strains [mm/m] over the period of 05.2014–08.2019, determined per the Knothe-Budryk theory (blue lines), with LDGDs locations (red lines).

groups 2, 3 and 4) presented in Fig. 4, which was measured using the InSAR method.

3.2. Subsidence velocity

The results of the surface subsidence velocity analysis are presented in charts (Fig. 6). They depict the mean surface subsidence velocity in the area of the generated discontinuous deformations. Twelve charts were prepared for the 12 LDGD groups per Table 1. The subsidence velocity in the month when a given group of discontinuities was detected is marked in red.

The LDGD reactivation phenomenon occurred in deformation groups 1 and 9. This means that the first LDGDs in group 1 manifested themselves around August 2015, when the mean subsidence velocity was 6 mm/month. However, reactivation occurred three-and-a-half years later, in March 2019. The subsidence velocity was much greater by that time and amounted to 34 mm/month. In group 9, reactivation occurred already after a month. The first LDGDs appeared around July 2017, with more occurring already around August 2017. The surface subsidence velocity in July 2017 was 16 mm/month, whereas in August 2017 it was 12 mm/month. The dates presented in Table 1 and marked on the charts are the dates of LDGD field measurements. It can therefore be assumed that the deformations had occurred earlier. In this context, it should be noted that the surface subsidence velocities in the months when the LDGDs were measured are not the greatest in the entire analysed cycle. Nevertheless, an acceleration of the surface subsidence can be observed in the months preceding the deformation measurements (in the months of their potential appearance). The greatest such difference concerned the LDGDs of group 10. The surface subsidence velocity in the measurement month was 25 mm/month, whereas in the preceding month it was 96 mm/month. More detailed data regarding this issue is compiled in Table 3.

The most rapid surface subsidence was found in the area of deformation group 10 – with a mean velocity of 14 mm/month for the entire analysed cycle. The slowest subsidence was in the area of group 12–4 mm/month.

Fig. 6. Subsidence velocity (mm/month) for each LDGD group.

Table 3. Detailed information about subsidence velocity in the area of LDGDs groups.

Group	Velocity in the measurement month	Velocity in the months preceding the measurement
2	10.2015: 7 mm/month	09.2015: 8 mm/month
		08.2015: 15 mm/month
3	04.2016: 8 mm/month	03.2016: 7 mm/month
		02.2016: 10 mm/month
		01.2016: 13 mm/month
		12.2015: 16 mm/month
5	09.2016: 4 mm/month	08.2016: 9 mm/month
8	12.2018: 8 mm/month	11.2018: 9 mm/month
		10.2018: 29 mm/month
		09.2018: 15 mm/month
9	07.2017: 16 mm/month	06.2017: 19 mm/month
	08.2017: 12 mm/month	
10	12.2018: 25 mm/month	11.2018: 96 mm/month

4. Conclusions

The article presents an analysis of surface subsidence in the context of linear discontinuous ground deformation (LDGD) occurrence. Seventy eight cases of LDGD generation as a result of mining activity over the period of 2015–2019 were analysed using the example of a mine in the Upper Silesian Coal Basin in Poland. Satellite interferometry was used to determine the surface subsidence. The analysis concerned the locations of LDGDs relative to the conducted mining activity, the generated subsidence troughs and the horizontal strains, calculated per the Knothe-Budryk theory. The following conclusions can be drawn based on the performed analysis:

1. All the LDGDs occurred on the boundaries of extraction, and consequently on the boundaries of the subsidence trough and in the areas of the greatest horizontal strains. This fact corresponds to the LDGD related experience acquired to date, as described in the literature [1].
2. Calculations using satellite interferometry may constitute a means for the initial, preliminary control of undertaken mining-induced deformation reforecasting. The horizontal strain range determined based on the parameters recommended by the mining plant per the Knothe-Budryk theory differs from the subsidence trough calculated using the InSAR method. This is the first signal that the correctness of the conducted reforecasting needs to be examined.
3. Utilising satellite interferometry made it possible to analyse the surface subsidence velocities exactly in the areas of LDGD occurrence. Doing the same is impossible when employing classic surveying methods due to the limited measuring network.
4. The large quantity of spatial data provided by satellite interferometry may constitute valuable material complementing classic surveying measurements and theoretical assumptions.

Ethical statement

The authors state that the research was conducted according to ethical standards.

Funding body

This research was funded by Polish Ministry of Education and Science, Statutory Activity of the Central Mining Institute in Katowice no. 11351011-131.

Conflicts of interest

None declared.

References

[1] Kowalski A. Deformacje powierzchni na terenach górniczych kopalń węgla kamiennego. Katowice: Central Mining Institute; 2020.
[2] Whittaker DN, Reddish DJ. Subsidence, occurrence, prediction and control. Amsterdam – Oxford – New York – Tokyo: Elsevier; 1989.
[3] Kratzsch H. Bergschädenkunde. Deotscher Markscheider – verein e.v. Bochum. 1997.
[4] Klenczar T. Szkody górnicze. Stowarzyszenie mierniczych górniczych R. P. Katowice. 1939.
[5] Strzałkowski P, Szafulera K. Occurrence of linear discontinuous deformations in Upper Silesia (Poland) in conditions of intensive mining extraction - case study. Energies 2020;13(8): 1–16. https://doi.org/10.3390/en13081897.
[6] Kowalski A, Apanowicz B, Polanin P. New research on a case of linear discontinuous ground deformation (LDGD). J Sustain Min 2020;19(3):201–2011. https://doi.org/10.46873/2300-3960.1018.
[7] Grün E. Analyse und Prognose von Unsteitigkeiten als Folge bergbaubedingter Bodenbewegungen im linksniederrheinischen Steinkohlengebiet. Dissertation. RWTH Aachen; 1995.
[8] Kowalski A, Jędrzejec E, Gruchlik P. Linear discontinuous deformations of the surface in the upper silesian Coal Basin. Arch Min Sci 2010;55(2):331–46.
[9] Wen-Bing G, Er-Hu B, Da-Ming Y. High-intensity mining characteristics and its evaluation system of thick coal seam in China's coalmines. Transac Strata Mech Res Inst 2018;20(2): 147–58.
[10] Zhu H, He F, Zhang S, Yang Z. An integrated treatment technology for ground fissures of shallow coal seam mining in the mountainous area of south western China: a typical case study. Miner Res Manag 2018;34(1):119–38.
[11] Ferretti A. Satellite InSAR data: reservoir monitoring from Space. EAGE. Houten; 2014.
[12] Perski Z, Mróz M. Zastosowanie metod interferometrii radarowej InSAR do badania naturalnych ruchów powierzchni terenu w Polsce. Arch Fotogram Karto Teledet 2007;17b:613–24.
[13] Beladam O, Balz T, Mohamadi B, Abdalhak M. Using PSInSAR with sentinel–1 images for deformation of monitoring in northeast Algeria. Geosciences 2019;9:315.
[14] Wu Q, Jia C, Chen S, Li H. SBAS – InSAR based deformation detection of urban land, created from mega-scale mountain

excavation and valley filling in the loess plateau: the case study of Yan'an City. Rem Sens 2019;11:1673.
[15] Zhang S, Chen B, Gong H, Lei K, Shi M, Zhou C. Three-dimensional surface displacement of the eastern Beijing Plain, China, using ascending and descending Sentinel-1AB images and leveling data. Rem Sens 2021;13:2809.
[16] Chaabani C, Chini M, Abdelfattah R, Hostache R, Chokmani K. Flood mapping in a complex environment using bistatic TanDEM-X/TerraSAR-X InSAR coherence. Rem Sens 2018;10(12):1873.
[17] Suresh D, Yarrakula K. InSAR based deformation mapping of earthquake using Sentinel 1A imagery. Geocarto Int 2019; 35:559–68.
[18] Atzori S, Antonioli A, Tolomei C, De Novellis V, De Luca C, Monterroso F. InSAR full – resolution analysis of the 2017 – 2018 M>6 earthquakes in Mexico. Rem Sens Environ 2019: 234.
[19] Hay-Man NA, Ge L, Yan Y, Li X, Chang HC, Zhang K, et al. Mapping accumulated mine subsidence using small stack of SAR differential interferograms in the Southern coalfield of New South Wales, Australia. Eng Geol 2010;115:1–15.
[20] Chen B, Mei H, Li Z, Wang Z, Yu Y, Yu H. Retrieving three-dimensional large surface displacement in coal mining areas by combining SAR Pixel Offset measurements with an improved mining subsidence model. Rem Sens 2021; 13:2541.
[21] Przyłucka M, Graniczny M. Kompleksowe wykorzystanie przetworzeń DInSAR i PSInSAR w badaniu pionowych przemieszczeń terenu w wybranych rejonach GO. Przeglad Gorn 2015;3:80–8.
[22] Malinowska A, Witkowski W, Hejmanowski R, Chang L, Van Leijen F, Hanssen R. Sinkhole occurrence monitoring over shallow abandoned coal mines with satellite–based persistent scatterer interferometry. Eng Geol 2019;262:1–13.
[23] Milczarek W, Blachowski J, Grzempowski PK. Application of PSInSAR for assessment of surface deformations in post-mining area – case study of the former Walbrzych hard coal basin (SW Poland). Acta Geodyn Geomater 2017;1:41–52.
[24] Apanowicz B. Linear discontinuous ground deformation detection based on coherence analysis of pre and post event radar image pairs. J Appl Geodes 2021. online publication. https://doi.org/10.1515/jag-2021-0036.
[25] Knothe S. Równanie profilu ostatecznie wykształconej niecki osiadania. Arch Gorn Hut 1953;1(1):22–38.
[26] Knothe S. Prognozowanie wpływów eksploatacji górniczej. Śląsk. Katowice; 1984.
[27] Berardino P, Fornaro G, Lanari R, Sansosti E. A new algorithm for surface deformation monitoring based on small baseline differential SAR interferograms. IEEE Trans Geosci Rem Sens 2002;40(11).
[28] Goldstein RM, Zebker H, Werner CL. Satellite radar interferometry: two-dimensional phase unwrapping. Radio Sci 1988;23(4):713–20.
[29] Sandwell D, Mellors R, Tong X, Wei M, Wessel P. Open radar interferometry software for mapping surface deformation. Eos Trans 2011;92(28).
[30] Jędrzejec E. 32-bitowa aplikacja Szkody 4.0 do prognozowania poeksploatacyjnych deformacji górotworu. Konferencja nt. Problemy ochrony terenów górniczych. Prace Naukowe GIG 2002;41:193–200.